Supplementary Material for: Dynamical Onset of Light-Induced Unconventional Superconductivity – a Yukawa-Sachdev-Ye-Kitaev study

Lukas Grunwald,[1,2,*] Giacomo Passetti,[1] and Dante M. Kennes[1,2,†]

[1] *Institut für Theorie der Statistischen Physik, RWTH Aachen University and JARA-Fundamentals of Future Information Technology, 52056 Aachen, Germany*
[2] *Max Planck Institute for the Structure and Dynamics of Matter, Center for Free-Electron Laser Science (CFEL), Luruper Chaussee 149, 22761 Hamburg, Germany*

(Dated: September 11, 2023)

CONTENTS

EXACT SOLUTION OF YSYK ON THE KELDYSH CONTOUR

We derive the exact solution of the YSYK model on the Keldysh contour at large N. For completeness, we consider a slight generalization to the model introduced in the main text by considering spin non-diagonal interactions as well as a finite chemical potential. The Hamiltonian reads [1–3]

$$H = -\mu \sum_{i=1}^{N} c_{i\alpha}^{\dagger} c_{i\alpha} + \frac{1}{2} \sum_{k=1}^{N} \left(\pi_k^2 + \omega_0^2 \phi_k^2\right) + \frac{1}{N} \sum_{ij} \sum_{k} f(t) \tilde{g}_{ijk} \phi_k \, c_{i\alpha}^{\dagger} (\sigma_{\alpha\beta}^{\mathrm{x}}) c_{j\beta}, \tag{1}$$

where $\sigma_{\alpha\beta}^{\mathrm{x}}, x = 0, \ldots, 3$ denotes the Pauli-matrices and $f(t)$ a generic time dependent function. We will derive the general solution of Eq. (1) and restrict to our specific model with $\mathrm{x}, \mu = 0$ in the end. The starting point is the path-integral on the Keldysh-contour [4, 5]. For the YSYK model, the associated action appearing in the generating functional $Z = \int \mathcal{D}[\bar{\psi}, \psi] \mathcal{D}[\phi] \exp\{iS[\psi, \phi]\}$ reads

$$S[\psi, \phi] = S_0[\psi, \phi] + S_{\mathrm{int}}[\psi, \phi], \tag{2}$$

$$S_0[\psi, \phi] = \int_{\mathcal{C}} \left\{ \sum_i \bar{\psi}_{i\alpha}(t) \big(i\partial_t + \mu\big) \psi_\alpha(t) + \frac{1}{2} \sum_k \phi_k(t) \big(-\partial_t^2 - \omega_0^2\big) \phi_k(t) \right\}, \tag{3}$$

$$S_{\mathrm{int}}[\psi, \phi] = -\frac{1}{N} \int_{\mathcal{C}} \sum_{ijk} f(t) \tilde{g}_{ij,k} \phi_k(t) \bar{\psi}_{i\alpha}(t) (\sigma_{\alpha\beta}^{\mathrm{x}}) \psi_{j\beta}(t). \tag{4}$$

We imply a summation over repeated Greek indices and use the shorthand $\int_{\mathcal{C}^{(\prime)}} (\dots) = \int_{\mathcal{C}} \mathrm{d}t^{(\prime)} (\dots)$ for integrals over the Keldysh-contour $\mathcal{C} = \mathcal{C}_+ \cup \mathcal{C}_-$, which consists of forward branch $\mathcal{C}_+$, running from $t_0 \to \infty$ and backward branch $\mathcal{C}_-$ running back from $\infty \to t_0$. We assume no initial correlations and set $t_0 \to -\infty$ [4, 5], which is sufficient for the non-equilibrium protocols we analyze in this work (see below).

From the non-interacting action S_0, we can directly extract the free fermionic and bosonic contour propagators

$$(G_0^{-1})_{\alpha\beta}(t,t') = \big[i\partial_t + \mu\big]\delta(t,t')\delta_{\alpha\beta}, \qquad D_0^{-1}(t,t') = \big[-\partial_t^2 - \omega_0^2\big]\delta(t,t'), \tag{5}$$

with $\int_{\mathcal{C}'}\delta(t,t') = 1$. Next we execute the disorder average over the interaction vertices $g_{ij,k} \in$ GOE (Gaussian-Orthogonal-Ensemble [6]), where for each bosonic index k, $g_{ij,k}$ represents a random matrix in the indices i,j. The GOE is an ensemble of symmetric random matrices g_{ij} (suppress bosonic index k), which is defined over the mean $\overline{g_{ij}} = 0$ and the variance $\overline{g_{ij}g_{km}} = (\delta_{ik}\delta_{jm} + \delta_{im}\delta_{jk})g^2$ of the matrices. The probability density and measure read

$$\rho(g) \sim \exp\left(-\frac{1}{4g^2}\,\mathrm{Tr}\big(g^2\big)\right), \qquad d\mu(g) \sim \prod_{i\leq j} d(g_{ij}), \tag{6}$$

so that the evaluation of the disorder average reduces to calculating Gaussian integrals (no replica trick is needed in the Keldysh formalism [4]). The resulting disorder averaged action reads

$$\begin{aligned} iS_{\mathrm{avg}}[\psi,\phi] = &\int_{\mathcal{C}}\left\{\sum_i \bar\psi_{i\alpha}(t)\big(i\partial_t+\mu\big)\psi_\alpha(t) + \frac{1}{2}\sum_k \phi_k(t)\big(-\partial_t^2-\omega_0^2\big)\phi_k(t)\right\} \\ &+\frac{g^2}{2N^2}\int_{\mathcal{C}}\int_{\mathcal{C}'} f(t)f(t')\sum_k \phi_k(t)\phi_k(t')\left\{\left[\sum_i\big(\psi_{i,\beta}\bar\psi_{i,\alpha'}\big)(t,t')\right]\big(\sigma^{\mathrm{x}}_{\alpha',\beta'}\big)\left[\sum_i\big(\psi_{j,\beta'}\bar\psi_{j,\alpha}\big)(t',t)\right]\big(\sigma^{\mathrm{x}}_{\alpha,\beta}\big)\right. \\ &\left. -\left[\sum_i\big(\bar\psi_{i,\alpha}\bar\psi_{i,\alpha'}\big)(t,t')\right]\big(\sigma^{\mathrm{x}}_{\alpha',\beta'}\big)\left[\sum_j\big(\psi_{i,\beta'}\psi_{i,\beta}\big)(t',t)\right]\big(\sigma^{\mathrm{x}}_{\alpha,\beta}\big)\right\}. \end{aligned} \tag{7}$$

Note the appearance of anomalous terms $\sim \psi_\alpha(t)\psi_\beta(t')$, which give rise to superconductivity and which are entirely due to $g_{ij,k} \in$ GOE being real. For complex $g_{ij,k} \in$ GUE (Gaussian-Unitary-Ensemble), like in the SYK model [7], we would obtain Eq. (7), but without the anomalous contributions. Next, we introduce the site averaged contour Greens functions and corresponding self-energies (Lagrange-multipliers) as dynamical mean-fields via fat-unities

$$1 = \int \mathcal{D}[\Sigma,G]\exp\left(N\int_{\mathcal{C}}\int_{\mathcal{C}'}\Sigma_{\alpha\beta}(t,t')\left\{G + \frac{i}{N}\sum_i \psi_i\bar\psi_i\right\}_{\beta\alpha}(t',t)\right), \tag{8}$$

$$1 = \int \mathcal{D}[\Pi,D]\exp\left(-\frac{N}{2}\int_{\mathcal{C}}\int_{\mathcal{C}'}\Pi(t,t')\left\{D + \frac{i}{N}\sum_k \phi_k\phi_k\right\}(t',t)\right), \tag{9}$$

$$1 = \int \mathcal{D}[\bar\phi,F]\exp\left(\frac{N}{2}\int_{\mathcal{C}}\int_{\mathcal{C}'}\bar\phi_{\alpha\beta}(t,t')\left\{F + \frac{i}{N}\sum_i \psi_i\psi_i\right\}_{\beta\alpha}(t',t)\right), \tag{10}$$

$$1 = \int \mathcal{D}[\phi,\bar F]\exp\left(\frac{N}{2}\int_{\mathcal{C}}\int_{\mathcal{C}'}\phi_{\alpha\beta}(t,t')\left\{\bar F + \frac{i}{N}\sum_i \bar\psi_i\bar\psi_i\right\}_{\beta\alpha}(t',t)\right). \tag{11}$$

The signs and prefactors are chosen in anticipation of obtaining Dyson equations (see below). Using the dynamical mean-fields, one finds for the interaction part ($\sim g^2$) of the averaged action

$$\frac{iS_{\mathrm{avg,int}}}{N} = -\frac{ig^2}{2}\int_{\mathcal{C}}\int_{\mathcal{C}'} f(t)f(t')D(t,t')\,\mathrm{tr}\Big[G_{\cdot,\cdot}(t,t')\sigma^{\mathrm{x}}G_{\cdot,\cdot}(t',t)\sigma^{\mathrm{x}} - \bar F_{\cdot,\cdot}(t,t')\sigma^{\mathrm{x}}F_{\cdot,\cdot}(t',t)(\sigma^{\mathrm{x}})^{\mathrm{T}}\Big], \tag{12}$$

where the tr[...] is to be taken over the spin indices. The $\psi,\bar\psi$ and ϕ fields are now decoupled and can be integrated out separately after taking into account the self-energy contributions from the fat unities. This process is straight forward in the bosonic case

$$\int \mathcal{D}[\phi]\exp\left\{i\int_{\mathcal{C}}\int_{\mathcal{C}'}\sum_k \phi_k(t')\big[D_0^{-1}(t,t') - \Pi(t,t')\big]\phi_k(t')\right\} \sim \exp\left\{-\frac{N}{2}\log\det\big[D_0^{-1} - \Pi\big]\right\}. \tag{13}$$

In the fermionic sector, the action contains both normal $\sim \bar\psi_\alpha\psi_\beta$ and anomal $\sim \psi_\alpha\psi_\beta$ contributions, the latter stemming from the fat unities Eqs. (10) and (11). We introduce Nambu vectors $\vec\psi_i = (\psi_{i,\uparrow},\psi_{i,\downarrow},\bar\psi_{i,\uparrow},\bar\psi_{i,\downarrow})$ to rewrite the remaining fermionic action as a Grassman-Gaussian integral

$$\int \mathcal{D}[\vec\psi]\ \exp\left\{\frac{i}{2}\int_{\mathcal{C}}\int_{\mathcal{C}'}\sum_i \vec\psi_i^\dagger(t)\big[\tilde{\boldsymbol{G}}_0^{-1}(t,t') - \tilde{\boldsymbol{\Sigma}}(t,t')\big]\vec\psi(t')\right\} \tag{14}$$

$$\text{with}\quad \tilde{\boldsymbol{G}}_0^{-1}(t,t') = \begin{pmatrix} (G_0^{-1})_{\cdot,\cdot} & 0 \\ 0 & -(G_0^{-T})_{\cdot,\cdot} \end{pmatrix}(t,t'), \qquad \tilde{\boldsymbol{\Sigma}}(t,t') = \begin{pmatrix} \Sigma_{\cdot,\cdot} & \phi_{\cdot,\cdot} \\ \bar{\phi}_{\cdot,\cdot} & -\Sigma_{\cdot,\cdot}^{\mathrm{T}} \end{pmatrix}(t,t'). \tag{15}$$

Here we introduced the Nambu-Keldysh self-energy $\tilde{\boldsymbol{\Sigma}}(t,t')$ and free-propagator $\tilde{\boldsymbol{G}}_0(t,t')$ and understand the transpose as $A_{\alpha\beta}(t,t')^{\mathrm{T}} = A_{\beta\alpha}(t',t)$. Note that the integral-measure only contains $\vec{\psi}$ but not $\vec{\psi}^\dagger$, since the latter is just a rearrangement of the former. Hence, Eq. (14) is not an ordinary Grassman-Gaussian integral. For $M \in \mathrm{Skew}_n$ and Grassman fields $\vec{\theta} = (\theta_1, \dots, \theta_n)$ integrals of this type equate to [8]

$$\int \mathrm{d}\vec{\theta} \exp\left(-\frac{1}{2}\vec{\theta}^{\mathrm{T}} M \vec{\theta}\right) = \begin{cases} \mathrm{Pf}(M) & n \text{ even} \\ 0 & n \text{ odd}\,. \end{cases} \tag{16}$$

Equation (14) can be brought into exactly this form by permuting elements in $[\dots]$, and we always have even n because of the 4-component Nambu vectors. Using Eq. (16) and reversing the permutation in the $\log \mathrm{Pf}[\dots]$ term, we find

$$\int \mathcal{D}[\vec{\psi}]\ \exp\left\{\frac{i}{2}\int_{\mathcal{C}}\int_{\mathcal{C}'} \sum_i \vec{\psi}_i^\dagger(t)\left[\tilde{\boldsymbol{G}}_0^{-1}(t,t') - \tilde{\boldsymbol{\Sigma}}(t,t')\right]\vec{\psi}(t')\right\} \sim \exp\Big\{N \log \mathrm{Pf}\left[\tilde{\boldsymbol{G}}_0^{-1} - \tilde{\boldsymbol{\Sigma}}\right]\Big\}. \tag{17}$$

The resulting $G\Sigma$-action only depends on the dynamical mean fields $G, \Sigma, F, \phi, \bar{F}, \bar{\phi}$ and reads

$$\begin{aligned} \frac{iS_{G\Sigma}}{N} =& \log \mathrm{Pf}\left[\tilde{\boldsymbol{G}}_0^{-1} - \tilde{\boldsymbol{\Sigma}}\right] - \frac{1}{2}\log\det\left[D_0^{-1} - \Pi\right] + \frac{1}{2}\mathrm{Tr}\big(\tilde{\boldsymbol{\Sigma}} \star \tilde{\boldsymbol{G}}\big) - \frac{1}{2}\mathrm{Tr}\big(\Pi \star D\big) \\ &- \frac{ig^2}{2}\int_{\mathcal{C}}\int_{\mathcal{C}'} f(t)f(t')D(t,t')\,\mathrm{tr}\Big[G_{\cdot,\cdot}(t,t')\sigma^{\mathrm{x}}G_{\cdot,\cdot}(t',t)\sigma^{\mathrm{x}} - \bar{F}_{\cdot,\cdot}(t,t')\sigma^{\mathrm{x}}F_{\cdot,\cdot}(t',t)(\sigma^{\mathrm{x}})^{\mathrm{T}}\Big], \end{aligned} \tag{18}$$

where the $\mathrm{Tr}(\dots)$ is to be taken over all indices and times and where we arranged fermionic propagators $G, F, \bar{F}$ into the Nambu-Keldysh Greens function

$$\tilde{\boldsymbol{G}}(t,t') = \begin{pmatrix} G_{\cdot,\cdot} & F_{\cdot,\cdot} \\ \bar{F}_{\cdot,\cdot} & -G_{\cdot,\cdot}^{\mathrm{T}} \end{pmatrix}(t,t'). \tag{19}$$

The shorthand $(.\star.)$ abbreviates convolutions over the support of the functions involved, in this case the Keldysh-contour $\mathcal{C}$ as well as the matrix structure of the GF's.

The action is globally multiplied by N, such that in the large N limit, the exact solution can be obtained by evaluating the variation $\delta S_{G\Sigma}$. This yields equations of motion for the dynamical mean-fields. Similar to derivatives of $\log\det(\dots)$ terms, (functional) derivatives of Pfaffians can be calculated as [8]

$$\frac{1}{\mathrm{Pf}(A)}\frac{\partial \mathrm{Pf}(A)}{\partial A_{ij}} = \frac{1}{2}\,\mathrm{tr}\left[A^{-1}\frac{\partial A}{\partial A_{ij}}\right]. \tag{20}$$

Varying the action with respect to the self-energies $\Sigma, \phi, \bar{\phi}$ and Π, we obtain the contour Dyson equations [4, 5] for the Numbu-Keldysh GF's and the bosonic propagator respectively

$$\tilde{\boldsymbol{G}}(t,t') = \left(\tilde{\boldsymbol{G}}_0^{-1} - \tilde{\boldsymbol{\Sigma}}\right)^{-1}(t,t'), \qquad D(t,t') = \left(D_0^{-1} - \Pi\right)^{-1}(t,t'). \tag{21}$$

During the evaluation of the former we used $[\tilde{\boldsymbol{G}}_0^{-1} - \tilde{\boldsymbol{\Sigma}}]_{11}^{-1} = -[\tilde{\boldsymbol{G}}_0^{-1} - \tilde{\boldsymbol{\Sigma}}]_{22}^{-\mathrm{T}}$. The equations for the self-energies follow by varying $S_{G\Sigma}$ with respect to the Greens functions $G, F, \bar{F}, D$, resulting in

$$\Sigma_{\alpha\beta}(t,t') = ig^2 f(t)f(t')D(t,t')\left[\sigma^{\mathrm{x}}G_{\cdot,\cdot}(t,t')\sigma^{\mathrm{x}}\right]_{\alpha\beta}, \tag{22}$$

$$\phi_{\alpha\beta}(t,t') = -ig^2 f(t)f(t')D(t,t')\left[\sigma^{\mathrm{x}}F_{\cdot,\cdot}(t,t')(\sigma^{\mathrm{x}})^{\mathrm{T}}\right]_{\alpha\beta}, \tag{23}$$

$$\bar{\phi}_{\alpha\beta}(t,t') = -ig^2 f(t)f(t')D(t,t')\left[(\sigma^{\mathrm{x}})^{\mathrm{T}}\bar{F}_{\cdot,\cdot}(t,t')\sigma^{\mathrm{x}}\right]_{\alpha\beta}, \tag{24}$$

$$\Pi(t,t') = -ig^2 f(t)f(t')\,\mathrm{tr}\Big[G_{\cdot,\cdot}(t,t')\sigma^{\mathrm{x}}G_{\cdot,\cdot}(t',t)\sigma^{\mathrm{x}} - \bar{F}_{\cdot,\cdot}(t,t')\sigma^{\mathrm{x}}F_{\cdot,\cdot}(t',t)(\sigma^{\mathrm{x}})^{\mathrm{T}}\Big]. \tag{25}$$

Equations (22) to (25) determine the exact self-energies of the YSYK model on the Keldysh contour ($t, t' \in \mathcal{C}$). We additionally obtained them using a diagrammatic derivation as a consistency check. Note that this system of equations

only depends on the site averaged GF's and self-energies. This illustrates the self-averaging property, since the exact solution has no reference to the site indices of the original theory.

The hence derived equations contain both singlet and triplet pairing components. As in previous works on the YSYK model, we focus on the x = 0 case, where the model has a SU(2) symmetry. The presence of triplet superconductivity would spontaneously break this symmetry. Following [1, 2], we assume no spontaneous SU(2) symmetry breaking and will thus focus on singlet anomalous propagators. On the Keldysh contour this implies $F_{\cdot,\cdot} = F_\mathrm{s} i\sigma_y$ with $F_\mathrm{s} = \frac{F_{\uparrow\downarrow} - F_{\downarrow\uparrow}}{2}$. Further, due to the SU(2) symmetry, the normal GF and self-energy become spin independent, i.e. $G_{\cdot,\cdot}(t,t') = G(t,t')\sigma_0$ and $\Sigma_{\cdot,\cdot}(t,t') = \Sigma(t,t')\sigma_0$. Henceforth, we can work with reduced Nambu-vectors $\psi_i = (c_{i\uparrow}, c^\dagger_{i\downarrow})^\mathrm{T}$ and the associated contour GF's and self-energies ($t, t' \in \mathcal{C}$)

$$\boldsymbol{G}(t,t') = -\frac{i}{N}\sum_i \overline{\langle T_\mathcal{C}\{\psi_i(t)\psi_i^\dagger(t')\}\rangle} = \begin{pmatrix} G(t,t') & F_\mathrm{s}(t,t') \\ -\bar{F}_\mathrm{s}(t,t') & -G(t',t)\end{pmatrix} \tag{26}$$

$$\boldsymbol{\Sigma}(t,t') = \begin{pmatrix} \Sigma(t,t') & \phi_\mathrm{s}(t,t') \\ -\bar{\phi}_\mathrm{s}(t,t') & -\Sigma(t',t)\end{pmatrix}. \tag{27}$$

Equations (22) to (25) then simplify to the equations from the main text ($t, t' \in \mathcal{C}$)

$$\boldsymbol{G}(t,t') = \left(\boldsymbol{G}_0^{-1} - \boldsymbol{\Sigma}\right)^{-1}(t,t'), \tag{28}$$

$$D(t,t') = \left(D_0^{-1} - \Pi\right)^{-1}(t,t') \tag{29}$$

$$\boldsymbol{\Sigma}(t,t') = ig^2 f(t) f(t') D(t,t') \left[\sigma_3 \boldsymbol{G}(t,t')\sigma_3\right], \tag{30}$$

$$\Pi(t,t') = -ig^2 f(t) f(t') \,\mathrm{tr}\left[\sigma_3 \boldsymbol{G}(t,t')\sigma_3 \boldsymbol{G}(t',t)\right], \tag{31}$$

where $\boldsymbol{G}_0^{-1}(t,t') = \left[i\partial_t + \mu\boldsymbol{\sigma}_3\right]\delta(t,t')$. In order to solve Eqs. (28) to (31), we need to analytically continue them to real-times, and physical Greens functions $\boldsymbol{G}^\gtrless, D^\gtrless$ or $\boldsymbol{G}^{\mathrm{R/A/K}}, D^{\mathrm{R/A/K}}$. The latter are obtained by fixing the position of the contour times $t, t' \in \mathcal{C}$ on the Keldysh contour $t, t' \in \mathcal{C}_\pm$, viz. (similar for $D^\gtrless$) [5]

$$\boldsymbol{G}^>(t,t') = \boldsymbol{G}(t,t'), \quad \text{with} \quad t \in \mathcal{C}_-, t' \in \mathcal{C}_+, \tag{32}$$

$$\boldsymbol{G}^<(t,t') = \boldsymbol{G}(t,t'), \quad \text{with} \quad t \in \mathcal{C}_+, t' \in \mathcal{C}_-, \tag{33}$$

$$\boldsymbol{G}^\mathrm{R}(t,t') = \theta(t-t')\left(\boldsymbol{G}^> - \boldsymbol{G}^<\right)(t,t'), \tag{34}$$

$$\boldsymbol{G}^\mathrm{A}(t,t') = \theta(t'-t)\left(\boldsymbol{G}^< - \boldsymbol{G}^>\right)(t,t'), \tag{35}$$

$$\boldsymbol{G}^\mathrm{K}(t,t') = \left(\boldsymbol{G}^< + \boldsymbol{G}^>\right)(t,t'). \tag{36}$$

Using the Langreth theorems [5, 9], Eqs. (28) to (31) translate to a system of non-linear Volterra integro-differential equations for $\boldsymbol{G}^\gtrless$ and $D^\gtrless$ — the so called Kadanoff-Baym equations (KBe's)

$$\left(i\partial_t + \mu\boldsymbol{\sigma}_3\right)\boldsymbol{G}^\gtrless(t,t') = \left(\boldsymbol{\Sigma}^\mathrm{R} \star \boldsymbol{G}^\gtrless + \boldsymbol{\Sigma}^\gtrless \star \boldsymbol{G}^\mathrm{A}\right)(t,t') \equiv \boldsymbol{\mathcal{F}}_1^\gtrless(t,t'), \tag{37}$$

$$\boldsymbol{G}^\gtrless(t,t')\left(-i\overleftarrow{\partial}_{t'} + \mu\boldsymbol{\sigma}_3\right) = \left(\boldsymbol{G}^\mathrm{R} \star \boldsymbol{\Sigma}^\gtrless + \boldsymbol{G}^\gtrless \star \boldsymbol{\Sigma}^\mathrm{A}\right)(t,t') \equiv \boldsymbol{\mathcal{F}}_2^\gtrless(t,t'), \tag{38}$$

$$\left(-\partial_t^2 - \omega_0^2\right)D^\gtrless(t,t') = \left(\Pi^\mathrm{R} \star D^\gtrless + \Pi^\gtrless \star D^\mathrm{A}\right)(t,t') \equiv \mathcal{B}_1^\gtrless(t,t'), \tag{39}$$

$$D^\gtrless(t,t')\left(-\overleftarrow{\partial}_{t'}^2 - \omega_0^2\right) = \left(D^\mathrm{R} \star \Pi^\gtrless + D^\gtrless \star \Pi^\mathrm{A}\right)(t,t') \equiv \mathcal{B}_2^\gtrless(t,t'), \tag{40}$$

$$\boldsymbol{\Sigma}^\gtrless(t,t') = ig^2 f(t) f(t') D^\gtrless(t,t') \left[\sigma_3 \boldsymbol{G}^\gtrless(t,t')\sigma_3\right], \tag{41}$$

$$\Pi^\gtrless(t,t') = -ig^2 f(t) f(t') \,\mathrm{tr}\left[\sigma_3 \boldsymbol{G}^\gtrless(t,t')\sigma_3 \boldsymbol{G}^\lessgtr(t',t)\right], \tag{42}$$

where $(A \star B)(t,t') = \int_{t_0}^\infty A(t,\tau)B(\tau,t')\,\mathrm{d}\tau$ and matrix multiplications are implied. Due to the causality structure of the GF's, these equations can be integrated as an initial value problem (see next section).

In this work the initial conditions are fixed in the lower quadrant of the two-time plane $t, t' < 0$ as the equilibrium solution of Eqs. (37) to (42), i.e. for $f(t) \equiv$ const. In equilibrium the GF's only depend on time differences, allowing us to map the differential equations' [Eqs. (37) to (40)] onto algebraic equations in frequency space. There self-energies and Greens functions are connected by

$$\boldsymbol{G}^\mathrm{R}(\omega) = \frac{1}{(\omega + i0^+) + \mu\boldsymbol{\sigma}_3 - \boldsymbol{\Sigma}^\mathrm{R}(\omega)}, \qquad D^\mathrm{R}(\omega) = \frac{1}{(\omega + i0^+)^2 - \omega_0^2 - \Pi^\mathrm{R}(\omega)}. \tag{43}$$

Further $\boldsymbol{G}^{\mathrm{R}}(\omega), \boldsymbol{G}^{\mathrm{K}}(\omega)$ and $D^{\mathrm{R}}, D^{\mathrm{K}}$ are related by fluctuation dissipation theorems respectively [5]. Hence, Eq. (43) together with Eqs. (40) and (41) provides a closed, algebraic system of equations for the equilibrium GF's. It can be solved numerically using a fixed point iteration in combination with numerical Fourier transforms, which we evaluate using an interpolation based FFT-scheme [10]. The fixed point iteration is analog to the SYK model and previous studies of the YSYK model; see [1, 7, 11, 12] and references therein.

INTEGRATION OF KADANOFF-BAYM EQUATIONS

General Idea — In this section we discuss the general procedure – time stepping scheme – for solving Kadanoff-Baym equations. Since the general time-stepping is the same for bosons and fermions, we explain our scheme using the generic KBe's

$$\big[i\partial_t - h(t)\big]G^{\gtrless}(t,t') = \big(\Sigma^{\mathrm{R}} \star G^{\gtrless} + \Sigma^{\gtrless} \star G^{\mathrm{A}}\big)(t,t') \equiv \mathcal{F}_1^{\gtrless}(t,t'), \tag{44}$$

$$G^{\gtrless}(t,t')\big[-i\overleftarrow{\partial}_{t'} - h(t')\big] = \big(G^{\mathrm{R}} \star \Sigma^{\gtrless} + G^{\gtrless} \star \Sigma^{\mathrm{A}}\big)(t,t') \equiv \mathcal{F}_2^{\gtrless}(t,t'), \tag{45}$$

where $h(t)$ denotes the non-interacting Hamiltonian and the matrix structure is left implicit. The bosonic equations encountered in the last section are equivalent, apart from $\partial_t \to \partial_t^2$. We will comment on the implications of this below.

Because of the causality structure of $G^{\mathrm{R/A}}$ and $\Sigma^{\mathrm{R/A}}$, the r.h.s of the KBe's for $G^{\gtrless}(t,t')$ only depends on times smaller than $\max(t,t')$. Thus, providing initial conditions for $G^{\gtrless}(t,t')$ in some interval $t,t' \in (t_0,t_1)$, the KBe's can be integrated as an initial value problem [13]. Due to them being integro-differential equations, each time-step depends on *all* previous times via the history integrals $\mathcal{F}_1^{\gtrless}, \mathcal{F}_2^{\gtrless}$. A time-step is defined as advancing δt forward in time, naturally enforcing a time discretization $t_n = t_0 + n\delta t$. The different KBe's correspond to different directions in the (t,t')-plane and in order to perform a time-step, they need to be used in combination. This we illustrate in Fig. 1. Equation (44) propagates the Greens functions *down* [green, $G^{\gtrless}(t_1+\delta t, t' \in (t_0,t_1))$] and Eq. (45) propagates to the *right* [blue, $G^{\gtrless}(t \in (t_0,t_1), t_1+\delta t)$]. For the diagonal propagation [orange, $G^{\gtrless}(t_1+\delta t, t_1+\delta t)$] we subtract Eqs. (44) and (45) to obtain

$$i\partial_t G^{\gtrless}(t,t) = \big[h(t), G^{\gtrless}(t,t)\big] + \big(\mathcal{F}_1^{\gtrless} - \mathcal{F}_2^{\gtrless}\big)(t,t'). \tag{46}$$

Equations (44) to (46) allow the calculation of all points needed for further time steps (dotted line in Fig. 1). They can thus be used to propagate the GF's in the entire (t,t')-plane, given some initial conditions. The full integration of the KBe's yields $G^{\gtrless}(t,t')$ for $t,t' \in (t_0,t_{\max})$.

The bosonic equations [Eqs. (39) and (40)] have exactly the same analytical structure as Eqs. (44) and (45), and we can hence use the same scheme as outlined above with one caveat. Because of ∂_t^2 it is not possible to generate an equation for the diagonal, comparable to Eq. (46), which only contains a second order derivative. Instead, the diagonal is determined as a combination of propagation to the *right* and *down* [Eqs. (39) and (40)].

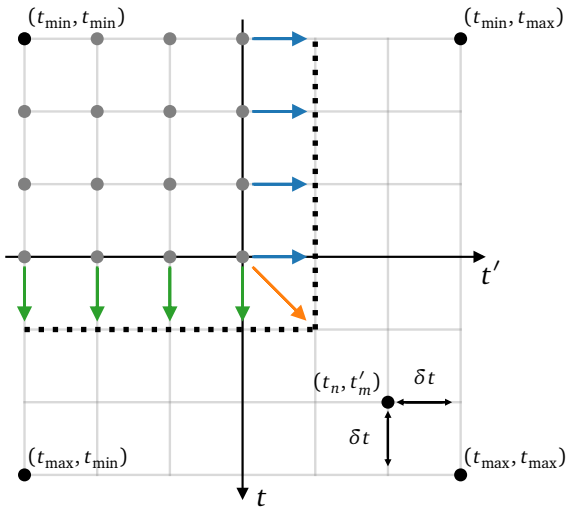

Figure 1. **KBe time stepping scheme**. Given $G^{>}(t,t'), G^{<}(t,t')$ on an initial interval $t,t' \in (t_0,t_1)$, here illustrated as gray dots, we can obtain the solution at all times by time-stepping with the KBe's. One time step comprises the calculation of the points indicated by the green $G^{\gtrless}(t_1+\delta t, t' \in (t_0,t_1))$, blue $G^{\gtrless}(t \in (t_0,t_1), t_1+\delta t)$, and orange $G^{\gtrless}(t_1+\delta t, t_1+\delta t)$ arrows, corresponding to the propagation with (44), (45), (46) respectively.

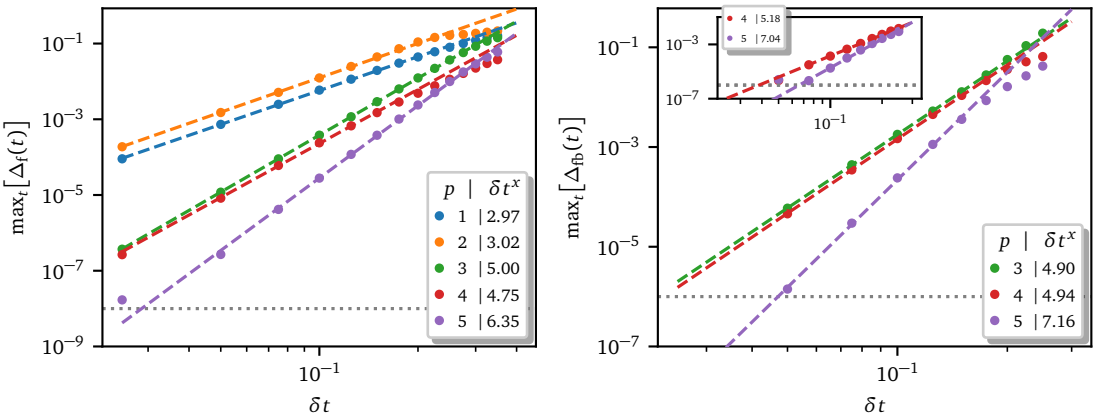

Figure 2. **Error scaling of equilibrium time evolution with KBe's**. Shown is the maximum error recorded during the time evolution. The expected scaling of the pth order methods is $\mathcal{O}(\delta t^{p+1})$. The dashed lines are linear fits to the log-data and the slope of this fit is shown in the right column of the legend. The gray dotted lines indicate the estimated accuracy of the equilibrium solution. *Left:* SYK model with $\beta = 10, \mu = 0.1, J = 1.2, K = 0.3$, see [17] for definition of model and parameters. The GF's are integrated from $t = 0$ to $t_{\max} = -t_{\min} = 100$. *Right:* YSYK model with $\beta = 1.2, \mu = 0.0, g = 1.0$. The GF's are integrated from $t = 0$ to $t_{\max} = -t_{\min} = 250$. The inset shows the scaling for the superconducting YSYK model with $\beta = 27.03, \mu = 0.0, g = 0.6$ with the same numerical parameters as the normal state.

Implementation — We solve the KBe's on the interval $[t_0, t_{\max}]$. Formally we have $t_0 \to -\infty$, but since GF's are decaying in time and since we are only interested in times $t \gg -\infty$, it is sufficient to consider $G(t, t')$ for $t, t' \in [t_{\min}, t_{\max}]$ where $t_{\min}$ is a numerical parameter, in which convergence has to be assured. We start the KBe time evolution at $t = 0$, thus providing initial conditions $G(t, t')$ for $t, t' < 0$ from the numerical iteration of the equilibrium KBe's; see end of last section.

Time steps are performed using a pth order linear multistep method (predictor-corrector) in combination with Gregory integration [14] for the history integrals, on a uniform time-grid $t_n = t_{\min} + n\delta t$; δt denoting the step-size. The two-time arguments of the Greens functions $G(t, t')$ hence become matrices with dimension $N_t \times N_t$, where $N_t = (t_{\max} - t_{\min})/\delta t$.

For first order electronic equations [Eqs. (37) and (38)] we use the pth order Adams-Moulten predictor-corrector method [15] and for second order bosonic equations [Eqs. (39) and (40)] we use the pth order Störmer's method [16]. The latter is a predictor-corrector scheme for differential equations only containing ∂_t^2, but no ∂_t. It is more accurate and numerically less expensive than mapping the second order equation onto two first order equations. The global integration error (full integration) for both pth order methods is $\mathcal{O}(\delta t^{p+1})$. The required computer memory for the KBe's scales as $\mathcal{O}(N_t^2)$, while the computational effort scales as $\mathcal{O}(N_t^3)$.

All data in this paper is generated with $p = 5$, i.e. an $\mathcal{O}(\delta t^6)$ scheme. Typical step sizes used in the integration are $\delta t = 0.02 - 0.05$, leading to matrix dimensions $N_t = 10.000 - 30.000$, depending on $t_{\max}$. Overall convergence of the results is most difficult to achieve at low temperatures and/or strong coupling g. For large couplings $g \geq 3$, a tiny $\delta t < 0.01$ is required to achieve numerical convergence, making the analysis in this regime numerically unfeasible.

Scaling of the method — Performing an equilibrium time evolution with the KBe's presents itself as a sensitive consistency check for the KBe solver. Using the equilibrium (eq) GF's as the initial condition for $t < 0$, we propagate the GF's to $t_{\max}$ using the KBe's. This is done without quench or time dependence in the Hamiltonian, i.e. with the equilibrium functionals $\Sigma[G]$. Since $G(t, t') = G(t - t')$ in equilibrium, the Gf's should not change along the propagation with the KBe's. We can thus compare the propagated GF's with the eq GF's at the end of the time evolution to measure the error of our numerical integration.

Since the implementation that calculates the eq GF's and the KBe code are completely separate, this provides a great consistency check, not only the KBe code, but also for the code that calculates the equilibrium solution of the system. The scaling analysis of this equilibrium propagation is shown in Fig. 2. The results for the propagation of the SYK equilibrium solution are shown on the left (see [17] for definition of the model) and for results for the normal state of the YSYK model on the right. The inset shows the scaling for the superconducting YSYK model. The YSYK model has not been considered in non-eq before, so that here the right panel presents a very sensitive consistency check for our novel implementation.

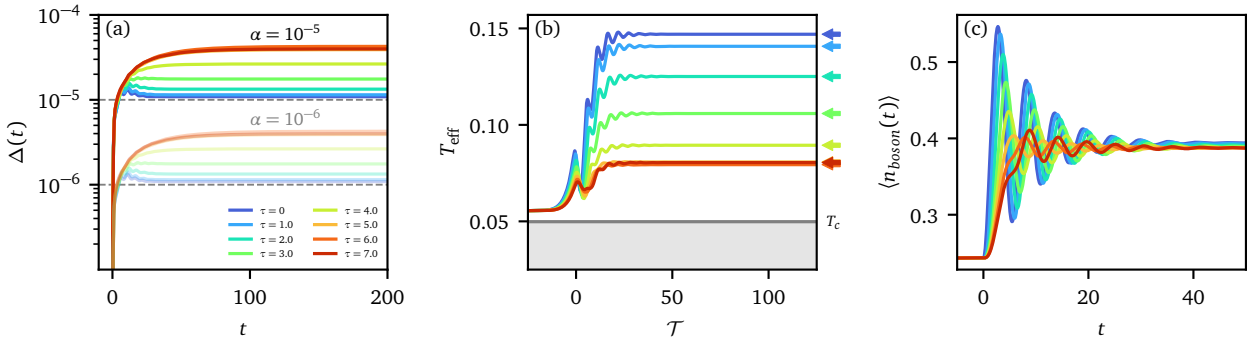

Figure 3. **Quenches across superconducting transition with finite ramping time** for $g = 0.75 \to 1.0$ with $\alpha = 10^{-5}$ (full lines) and $\alpha = 10^{-6}$ (desaturated lines; only distinguishable in the left panel). (a) The superconducting order parameter $\Delta(t)$ stays on the order of the symmetry breaking $\Delta(t) \sim \alpha$, implying that no superconductivity is induced. (b) After initial oscillations at early times, the effective temperature $T_{\rm eff}$ agrees with the instant temperature $T_{\rm inst}$ (color matched arrows), indicating thermalization at late times. Universally $T_{\rm eff}(t \to \infty) > T_{\rm c}$. (c) The bosonic ocuupation $\langle n_{\rm boson}(t)\rangle$ follows an analog behavior to the effective temperature, viz. oscillations at early times that relax in the long time limit.

QUENCH WITH FINITE RAMPING TIME

The inability to induce superconductivity following a quench across the phase boundary also persists when considering a finite ramp for the interaction quench. We study this for quenches from $g_{\rm i} = 0.75$ to $g_{\rm f} = 1.0$, where the finite ramping time τ is implemented as a linear ramp in $g_{ij,k} f(t)$ with

$$f(t) = g_{\rm i}\theta(-t) + \left(g_{\rm i} + \frac{g_{\rm f} - g_{\rm i}}{\tau} t\right)\theta(\tau - t) + g_{\rm f}\theta(t - \tau). \tag{47}$$

The exact dynamics for ramping times $\tau = 0, \ldots, 7$, where $\tau = 0$ corresponds to instant quenches, is shown in Fig. 3. Figure 3(a) plots the gap function $\Delta(t)$, Fig. 3(b) the effective temperature and Fig. 3(c) the bosonic occupation. A further increase in ramping time does not change the dynamics in any meaningful way, nor decrease the final effective temperature.

Analog to the instant quenches, the system relaxes to the new equilibrium state with an oscillatory dynamics. While it is possible to decrease the final temperature after the quench by increasing the ramp time τ, it does not seem to be possible to achieve $T_{\rm eff} < T_{\rm c}$, at least for the coupling considered here. The final temperature saturates for $\tau > 6$ [orange and red curves in Fig. 3(b)]. We universally find $\Delta(t) \sim \alpha$ [saturated and desaturated; Fig. 3(a)], implying that no transient superconductivity is induced.

At the largest ramping times $\tau \geq 6$, the system is 'locally thermal' during and after the quench, as we illustrate in Fig. 4, which shows the non-equilibrium occupation function $n(\mathcal{T}, \omega)$ for early and intermediate times. While for instant quenches and short ramps, the occupation function $n(\mathcal{T}, \omega)$ shows strong non-eq features ($n > 1$ or $n < 0$), these gradually decrease and vanish as the ramping times τ increases. At $\tau \geq 6$, the occupation function resembles as Fermi-distribution with time dependent temperature during the time evolution.

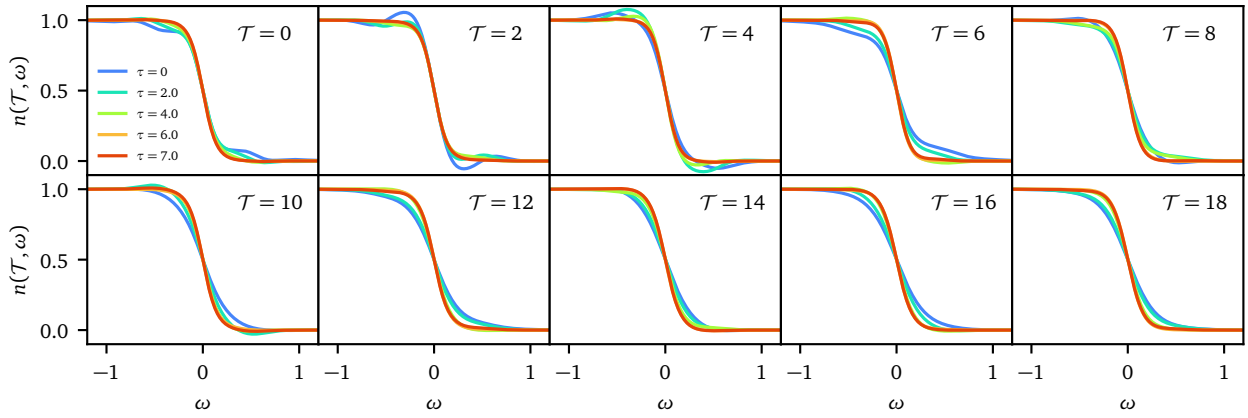

Figure 4. **Non-equilibrium ocuupation function $n(\mathcal{T},\omega)$ after quenches across superconducting transition** at fixed $\alpha = 10^{-5}$ for instant (blue) quenches and finite ramps. While instant quenches lead to strong non-equilibrium features in the non-equilibrium occupation function ($n > 1, n < 0$), these features gradually vanish as the ramping time increases.

THERMALIZATION TIME AND CRITICAL SLOWING DOWN

In the main text we remarked on the strong α dependence of the thermalization time t_*. Its functional dependence given by

$$t_*(\alpha) = t_{*,0} + C\log(1/\alpha), \tag{48}$$

with temperature dependent constants $C, t_{*,0} > 0$, as we illustrate in Fig. 5(a) (note the logarithmic x-axis). The turning-point time $\tilde{t}_*$, up to which the order parameter shows an exponential behavior, has exactly the same slope, but a different constant $t_{*,0} \to \tilde{t}_{*,0}$. The dynamical onset of superconductivity is hence exponentially activated in the strength of the symmetry breaking seed. This is readily understood via the exponential dynamics at early times $\Delta(t) \sim \exp(\Gamma t)$. The system inherently produces an exponentially growing seed, a short time after the initial symmetry breaking occurs. Hence, only providing an exponentially bigger initial seed can modify this self-propelled dynamics in a meaningful way.

Another interesting question is the parametric dependence of t_* on the initial temperature T of the normal state,

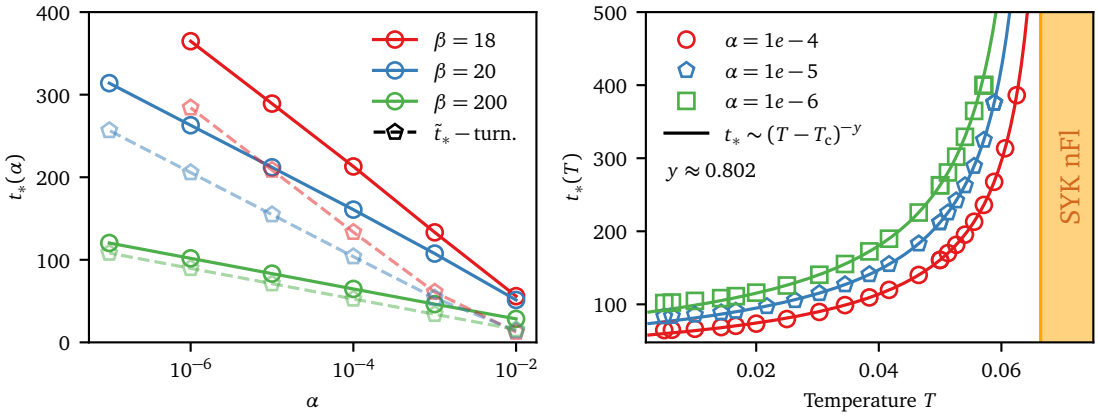

Figure 5. **Parametric dependence of thermalization time t_*.** (a) $t_*(\alpha)$ as a function of the symmetry breaking strength α for various temperatures. Both thermalization t_* (circle, full) and turning point $\tilde{t}_*$ (pentagon, dashes) follow a linear curve $t_*(\alpha) = t_{*,0} + C\log(1/\alpha)$, indicating that the relaxation is exponentially activated in α. (b) Temperature dependence of $t_*(T)$. Close to T_c (normal state; orange) we observe a critical slowing down, i.e. $t_*(T) \sim (T - T_c)^{-y}$ for which we extract the α independent exponent y by fitting $T \geq 0.03$. For temperatures $T \ll T_c$, the exact $t_*(T)$ deviates from this power-law form and saturates.

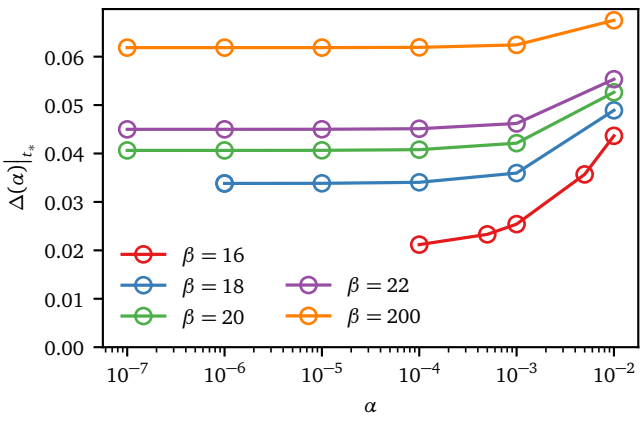

Figure 6. **Relaxed gap function** $\Delta(\alpha)|_{t_*}$ at thermalization time t_*, for $g = 1.0$ for different temperatures. Close to the superconducting transition temperature ($T_c \approx 1/15.1$) the relaxed Δ depends strongly on α, while deep within the superconducting phase it is much less sensitive. Since we want the final state to be independent of α on the scale of the plots, we must decrease it as we approach T_c. This, combined with the critical slowing down (see above), makes the numerical study of undercooled quenches close to T_c challenging.

which we analyze in Fig. 5(b). Here, we observe a critical slowing down of the relaxation dynamics as we approach the critical temperature T_c (orange region), i.e. $\lim_{T\to T_c} t_*(T) = \infty$, which is simply a different manifestation of $\lim_{T\to T_c} \Gamma(t) = 0$ discussed in the main text [18]. This feature is very intuitive, since the closer we get to T_c, the smaller the 'effective force' becomes, that pushes the system into a superconducting ground state. Right at T_c, the system is critical so that the restoring force vanishes and the thermalization time diverges.

While the dynamics is exponentially activated in the symmetry breaking strength, the thermalized value $\Delta(t > t_*)$ as well as the relaxation rate $\Gamma(T)$ are α-independent, for small enough α. That is desirable, since α is supposed to represent an infinitesimally small perturbation to the system that kick-starts our relaxation process, but does not affect the final state after relaxation (at least on the scale of the plots). This in turn means, that as we approach T_c, α needs to be become smaller for the final state to be α-independent, since the thermal equilibrium value of Δ continuously decreases to zero for $T \to T_c$. We illustrate this in Fig. 6. This in combination with the critical slowing down makes the analysis for $T \sim T_c$ numerically challenging.

UNDERCOOLING AT DIFFERENT COUPLING STRENGTHS

Here we comment on the undercooling dynamics at different coupling strengths g. The relaxation rate $\Gamma(T)$ extracted from the early time dynamics, is shown in Fig. 7 for a variety of different couplings (note the rescaled y-axis for better visibility). Close to T_c the prediction from overdamped Ginzburg-Landau theory (dashed) agrees well with the exact results, while the curves universally deviate from this behavior for stronger undercooling, where they show a saturation behavior. We observe that the dynamics is generally faster at stronger coupling. Further, we find that the oscillatory order parameter dynamics is most pronounced at weak and intermediate coupling $g \lesssim 1$, while the amplitude of the oscillations becomes strongly suppressed at strong coupling.

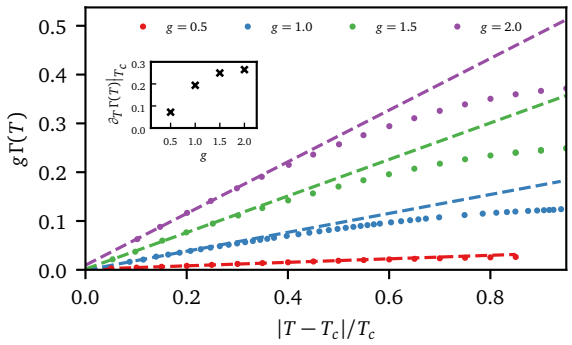

Figure 7. **Relaxation rate** $\Gamma(T)$ extracted from early time dynamics $\Delta(t) \sim e^{\Gamma(T)t}$ at $\alpha = 10^{-5}$ and different couplings g. The main panel shows $g \cdot \Gamma(T)$ (for better visibility) together with linear fits (dashed lines) $\Gamma(T) \sim c_1|T - T_c|/T_c + c_2$ to the exact data (dots). The inset illustrates the g-dependence for the slope of the linear fit $c_1 = \partial_T \Gamma(T)|_{T\to T_c}$. Note that $c_2 \approx 0$, indicating the critical slowing down. The dynamics is generally faster at stronger coupling $\partial_g c_1(g) > 0$, but like the critical temperature, saturates for $g \gtrsim 2$.

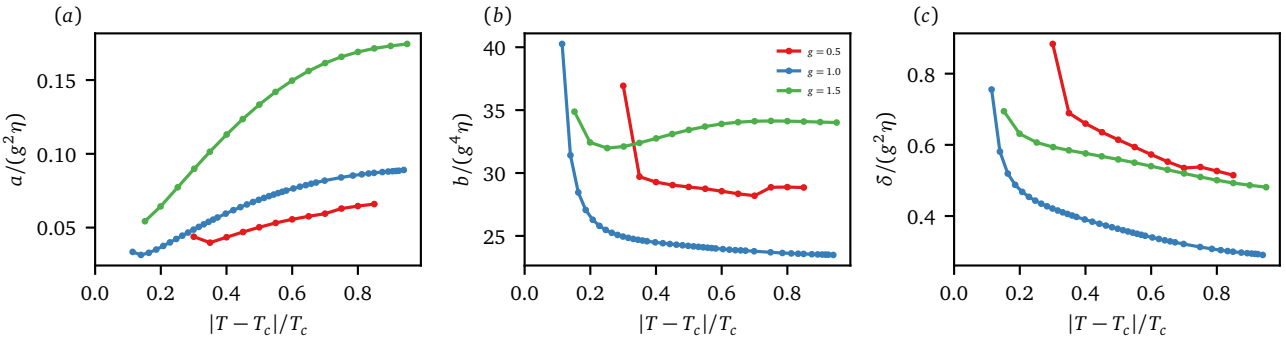

Figure 8. **Ginzburg-Landau parameters for undercooling protcol** at different couplings g. Axis are rescaled with the coupling strength g and critical temperatures T_c for better visualization. While the exact numerical values are sensitive to numerical details, the general trends appear to be universal.

GINZBURG-LANDAU PARAMETER FITS

We analyze the temperature and coupling dependence of the Ginzburg Landau theory (GL) parameters, mentioned in the main text. We obtained these from fits of the Ginzburg-Landau $\Delta_{\rm GL}(t)$ to the exact order parameter dynamics. Our Ginzburg Landau theory is defined by the Free energy $F_{\rm GL} = a\Delta_{\rm GL}^2 + b\Delta_{\rm GL}^4$ and dynamical equation

$$\eta\partial_t^2\Delta_{\rm GL}(t) + \delta\partial_t\Delta_{\rm GL}(t) = -\frac{\partial F_{\rm GL}}{\partial\Delta_{\rm GL}}, \qquad \Delta_{\rm GL}(t=0) = \alpha \tag{49}$$

which for $\eta \neq 0$ has to be solved numerically due to the non-linearity. Generally we find that the fitted parameters are very sensitive to small deviations in $\Delta(t)$, making an accurate numerical extraction difficult. The extracted values lead to $\Delta_{\rm GL}(t)$-curves, that on the scale of the plots, coincide with the exact $\Delta(t)$ dynamics, but one shouldn't put too much emphasis on the exact numerical values obtained here.

This procedure can nonetheless be used to determine the general trends for the GL parameters. The fits are obtained using the `BFGS` routine, implemented in `Optim.jl` [19], on $\Delta(t)$ and $\partial_t\Delta(t)$ together with `DifferentialEquations.jl` [20] for the numerical solution of the ODE's.

The extracted parameters are shown in Fig. 8 for different couplings g. Note that generally $a/\eta \to 0$ as $T \to T_c$ as expected [Fig. 8(a)]. In this limit $\delta/\eta \to \infty$ [Fig. 8(c)], implying that the dynamics becomes overdamped. We independently verified this by fitting GL theory with $\eta = 0$ to the exact numerical results close to T_c. This leads to excellent agreement with the exact data.

We generally find larger damping δ in the stronger coupling regime, with the rough scaling $\delta \sim \mathcal{O}(g^2)$; curves in the figure become of the same order of magnitude when applying this rescaling. Hence, in order to observe the oscillatory order parameter dynamics at strong coupling, a stronger undercooling is necessary.

* lukas.grunwald@mpsd.mpg.de
† dante.kennes@mpsd.mpg.de

[1] I. Esterlis and J. Schmalian, Phys. Rev. B Condens. Matter **100**, 115132 (2019).
[2] Y. Wang, Phys. Rev. Lett. **124**, 017002 (2020).
[3] W. Choi, O. Tavakol, and Y. B. Kim, SciPost Phys. **12**, 10.21468/scipostphys.12.5.151 (2022).
[4] A. Kamenev, *Field Theory of Non-Equilibrium Systems* (Cambridge University Press, Cambridge, 2011).
[5] J. Rammer, *Quantum Field Theory of Non-equilibrium States* (Cambridge University Press, Cambridge ; New York, 2007).
[6] G. Akemann, J. Baik, and P. Di Francesco, eds., *The Oxford Handbook of Random Matrix Theory*, 1st ed. (Oxford University Press, 2015).
[7] D. Chowdhury, A. Georges, O. Parcollet, and S. Sachdev, Reviews of Modern Physics **94**, 035004 (2022).
[8] J. Zinn-Justin, *Quantum Field Theory and Critical Phenomena*, 4th ed., International Series of Monographs on Physics No. 113 (Clarendon Press ; Oxford University Press, Oxford : New York, 2002).
[9] D. C. Langreth and J. W. Wilkins, Phys. Rev. B Condens. Matter **6**, 3189 (1972).
[10] Press,William H. and S. A. Teukolsky, Computers in Physics **3**, 91 (1989).
[11] X.-Y. Song, C.-M. Jian, and L. Balents, Physical Review Letters **119**, 216601 (2017).

[12] D. Valentinis, G. A. Inkof, and J. Schmalian, Correlation between phase stiffness and condensation energy across the non-Fermi to Fermi-liquid crossover in the Yukawa-Sachdev-Ye-Kitaev model on a lattice (2023), arxiv:2302.13134 [cond-mat].
[13] G. Stefanucci and R. van Leeuwen, *Nonequilibrium Many-Body Theory of Quantum Systems: A Modern Introduction* (Cambridge University Press, Cambridge, 2013).
[14] B. Fornberg, SIAM Rev. **63**, 167 (2021).
[15] J. C. Butcher, *Numerical Methods for Ordinary Differential Equations* (John Wiley & Sons, 2016).
[16] E. Hairer, S. P. Nørsett, and G. Wanner, *Solving Ordinary Differential Equations I Nonstiff Problems*, 2nd ed. (Springer, Berlin, 2000).
[17] C. Kuhlenkamp and M. Knap, Phys. Rev. Lett. **124**, 106401 (2020).
[18] P. C. Hohenberg and B. I. Halperin, Reviews of Modern Physics **49**, 435 (1977).
[19] P. K. Mogensen and A. N. Riseth, Journal of Open Source Software **3**, 615 (2018).
[20] C. Rackauckas and Q. Nie, Journal of Open Research Software **5**, 10.5334/jors.151 (2017).